Title: Predictive filtering of sensory response via orbitofrontal top-down input

Authors: Hiroaki Tsukano[1,2], Michellee M. Garcia[1,2], Pranathi R. Dandu[1,2], Hiroyuki K. Kato[1-5]*

Affiliations:

[1]Department of Psychiatry, University of North Carolina at Chapel Hill; Chapel Hill, 27599, USA.

[2]Neuroscience Center, University of North Carolina at Chapel Hill; Chapel Hill, 27599, USA.

[3]Carolina Institute for Developmental Disabilities, University of North Carolina at Chapel Hill; Chapel Hill, 27599, USA.

[4]Eaton-Peabody Laboratories, Massachusetts Eye and Ear; Boston, 02114, USA.

[5]Department of Otolaryngology - Head and Neck Surgery, Harvard Medical School; Boston, 02114, USA.

*Corresponding author. Email: hkato3@meei.harvard.edu

Abstract: Habituation is a crucial sensory filtering mechanism whose dysregulation can lead to a continuously intense world in disorders with sensory overload. While habituation is considered to require top-down predictive signaling to suppress irrelevant inputs, the exact brain loci storing the internal predictive model and the circuit mechanisms of sensory filtering remain unclear. We found that daily neural habituation in the primary auditory cortex (A1) was reversed by inactivation of the orbitofrontal cortex (OFC). Top-down projections from the ventrolateral OFC, but not other frontal areas, carried predictive signals that grew with daily sound experience and suppressed A1 via somatostatin-expressing inhibitory neurons. Thus, prediction signals from the OFC cancel out behaviorally irrelevant anticipated stimuli by generating their “negative images” in sensory cortices.

Main Text:

Throughout our lives, we are constantly exposed to a flood of sensory information from the external world. However, only a small fraction of this information reaches our conscious perception and triggers behavioral responses. This remarkable filtering, which prioritizes inputs with expected meaningful outcomes while ignoring others, arises from our brain's ability to build internal models of the world (*1–3*). These models are continuously trained through our lifetime experiences and dictate predictive relationships between sensory objects in the world. The inability to build such predictive models, and thus to apply appropriate sensory filters, is a hallmark of mental disorders such as obsessive-compulsive disorder (*4*, *5*), schizophrenia (*6*), and most notably, autism spectrum disorders (ASD)(*7–10*).

One fundamental form of such sensory filtering is habituation, the brain's ability to ignore familiar, inconsequential stimuli (*11–13*). Habituation operates through multitudes of mechanisms, allowing animals to adapt to the statistical structures of their sensory environments over a wide range of timescales. While previous research primarily focused on mechanisms for short-term plasticity lasting from milliseconds to seconds, known as "stimulus-specific adaptation" (*14–21*), habituation also extends to longer periods—days or even weeks (*22–26*)—as evidenced by the gradual reduction in our sensitivity to perfumes or traffic noise. This long-term habituation is particularly relevant for understanding the pathology of filtering deficits, as a lack of accumulated habituation to daily sensory objects throughout one's life could result in a persistently intense sensory world (*27–32*).

Contrary to the widely held belief that habituation is the "simplest form of learning," accumulating evidence has challenged this perceived simplicity. Classical internal model-free mechanisms, such as sensory receptor fatigue, homosynaptic depression, and the short-term dynamics of inhibitory neuron firing, fail to fully account for several key characteristics of habituation. These characteristics include its persistence over weeks, capacity to process complex stimuli involving multiple sensory channels,

context-dependence (*33–35*), and disruption by anesthesia (*36*, *37*). These observations have prompted theories suggesting that habituation is associative and governed by top-down regulation informed by internal models of the external world (*11*, *29*, *36*, *38*, *39*).

Two competing hypotheses have been proposed to explain the top-down circuit mechanisms of long-term sensory habituation. The predictive negative image hypothesis posits that initially strong sensory responses are gradually canceled as the top-down predictive signal grows (Fig. 1A, left, and fig. S1A). Supporting this hypothesis, somatostatin-expressing inhibitory neurons (SST cells) in sensory cortices increase their sensory responses over days of stimulus exposure (*40–42*), providing neuronal substrates for the generation of a 'negative image' of the stimulus. An alternative is the novelty (or prediction error) hypothesis, which assumes that sensory-evoked activity is weak by default and is amplified by a top-down novelty signal upon the animal's first encounter with a stimulus (Fig. 1A, right)(*43–46*). This view proposes that the activation of vasoactive intestinal peptide-expressing inhibitory neurons (VIP cells) by the novelty signal disinhibits pyramidal neurons, and habituation occurs as the novelty signal wanes over time.

Despite their fundamentally distinct mechanisms, activity measurements in sensory cortices alone have failed to differentiate these hypotheses. Due to the reciprocal connections between SST and VIP cells, both models predict similar neuronal dynamics during habituation: an increase in SST cell activity and a decrease in VIP and pyramidal cell activity. To discriminate between these theories, we sought to identify the source of the top-down input to A1 during daily sensory habituation and determine the 'default' sensory responses by removing the top-down signal.

A1 neurons show sound-specific habituation across days

We induced sensory habituation in awake, head-fixed mice through repeated exposure to tones over five days (5–9 seconds pure tones, 7–16 seconds inter-trial interval, 70 dB SPL, 200 trials/day) (Fig. 1, B and

C). To track the activity of the same A1 layer 2/3 (L2/3) neural ensembles across days, we conducted chronic two-photon calcium imaging. We first located A1 by intrinsic signal imaging (*47*) and virally expressed GCaMP6s in the A1 of wild-type or VGAT-Cre × Ai9 mice. Three weeks after virus injection and optical window implantation, we recorded sound-evoked activities from 5,483 L2/3 neurons in 20 mice. We chose a fixed tone frequency for each mouse and imaged the corresponding tonotopic domain in A1, where we tracked the same neural ensembles throughout the experiment. Across days of sound exposure, we observed clear habituation in tone responses, characterized by reduced excitation and increased suppression in a sound-specific manner (Fig. 1, D to H, fig. S2, A to C, and fig. S3), consistent with previous studies (*40*, *41*). Given indistinguishable results between experiments imaging all L2/3 neurons and those imaging only $VGAT^{-}$ pyramidal neurons, data from both experiments were combined and treated as A1 pyramidal cells (fig. S2, D to G).

We observed two timescales of habituation: within-day habituation, which repeated daily across trials, and across-day habituation, which built up over multiple days (Fig. 1, I and J). To better understand the relationship between these plasticity timescales, we projected high-dimensional population dynamics onto the axes defined by within-day and across-day changes. Notably, these two habituation mechanisms represented nearly orthogonal axes in the high-dimensional space (78.2 degree; Fig. 1K), indicating that across-day habituation is not simply the accumulated effect of within-day habituation. Within-day habituation markedly attenuated sound onset responses, whereas across-day habituation was greater during the sustained phase of tones (5 seconds after onset), implying two independent mechanisms for auditory habituation (Fig. 1, G, L, and M, and Supplementary Text). This difference in kinetics supports the role of slow, top-down predictive filtering in across-day habituation, while within-day habituation may be driven by faster, bottom-up mechanisms.

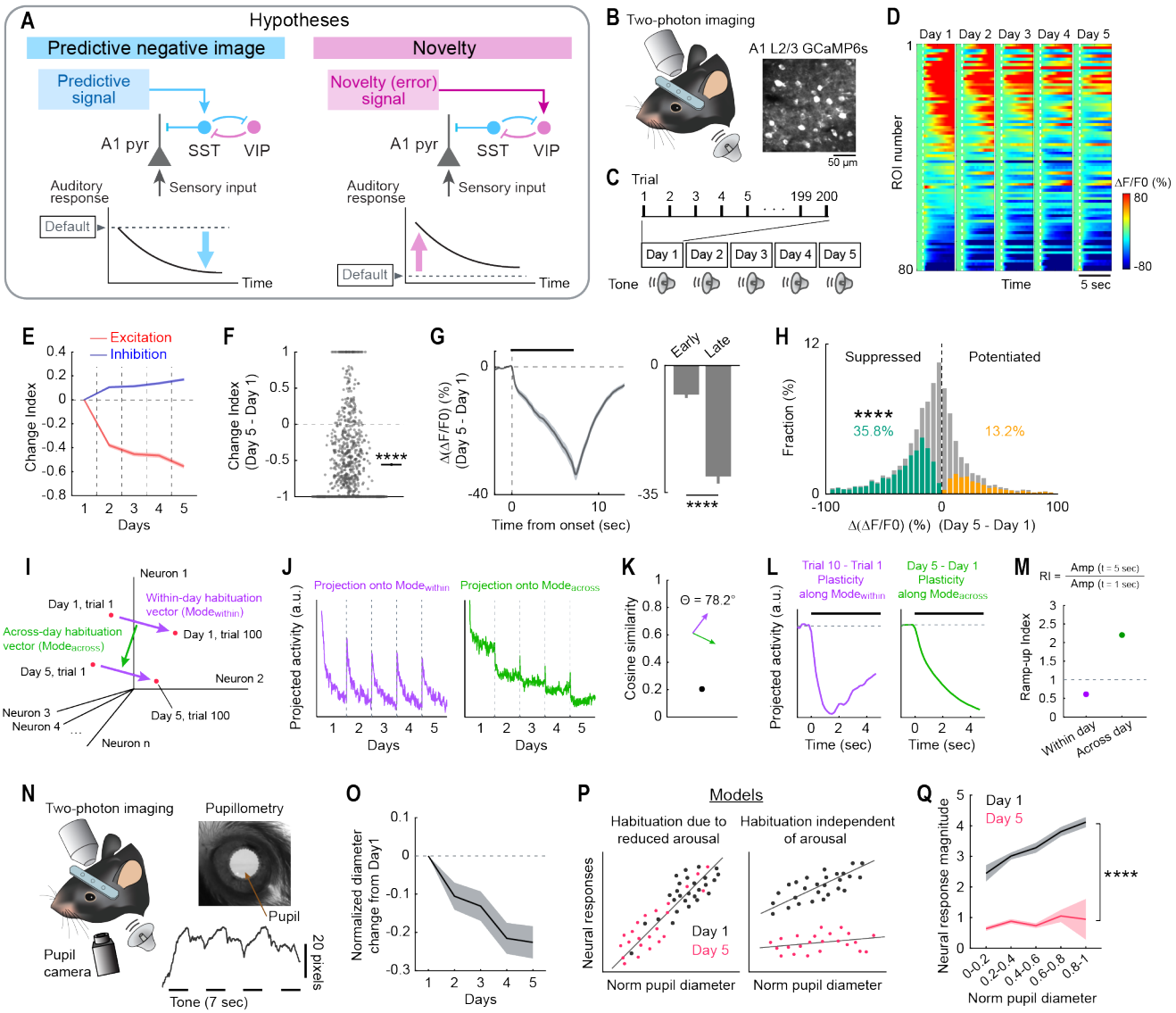

Fig. 1. Inactivation of OFC reverses across-day habituation in A1. (**A**) Schematics illustrating two theories explaining sensory habituation by top-down predictive mechanisms. (**B**) Representative two-photon image of A1 L2/3 neurons expressing GCaMP6s. (**C**) Schematic illustrating the five-day auditory habituation paradigm. (**D**) Heatmaps of sound-evoked responses in neurons imaged across five days in a representative mouse. Neurons are sorted by their responses on Day 1. (**E**) Average (solid line) and SEM (shading) of the Change Index for excitatory (red) and inhibitory (blue) sound-evoked responses across days. *n* = 20 mice. (**F**) Change Index of excitatory responses in individual neurons on Day 5 compared to Day 1 across all mice. Black lines on the right represent mean ± SEM. *n* = 879 responsive neurons. ****$P = 1.6 \times 10^{-66}$ (two-sided Wilcoxon signed-rank test). (**G**) Left: Change in sound-evoked response traces from Day 1 to Day 5 averaged across all significantly excited cells. Black bar: sound. Right: The amplitudes of the difference trace at 1 and 7 seconds after sound onset. ****$P = 1.4 \times 10^{-65}$ (two-sided Wilcoxon signed-rank test). (**H**) Histograms of changes in response magnitudes in all neurons. Orange and green bars show neurons with significant increase and decrease. ****$P = 4.3 \times 10^{-138}$ (Fisher's exact test). (**I**) Schematic illustrating vectors representing within-day habituation (purple: $Mode_{within}$) and across-day habituation (green: $Mode_{across}$) within

a high-dimensional space. Each dimension corresponds to the response magnitudes of individual neurons. (**J**) Projection of trial-to-trial sound-evoked A1 ensemble activity dynamics onto the $Mode_{within}$ (left) and $Mode_{across}$ (right) vectors. Data points represent individual trials (100 trials × 5 days). Ensemble activity patterns repeated fast daily plasticity along the $Mode_{within}$ axis, while they show continuous slow plasticity along the $Mode_{across}$ axis across five days. *n* = 20 mice, 2,398 cells imaged throughout the five days. (**K**) Cosine similarity between $Mode_{within}$ and $Mode_{across}$, indicating a nearly orthogonal relationship. (**L**) Left: Change in sound-evoked ensemble activity along $Mode_{within}$ from Trial 1 to Trial 10, demonstrating prominent within-day, across-trial habituation around the tone onset. Right: Change in sound-evoked ensemble activity along $Mode_{across}$ from Day 1 to Day 5. Across-day habituation slowly ramps up during the sustained tone. (**M**) Summary data showing the Ramp-up Index for across-day plasticity (Day 1 to Day 5) and within-day plasticity (Trial 1 to Trial 10). (**N**) Top left: Schematic illustrating pupil monitoring during two-photon calcium imaging. Top right: Representative image from a pupil camera. Bottom right: Representative pupil diameter dynamics during sound presentations. Black lines indicate tone timings. (**O**) Change in normalized pupil diameter from Day 1. *n* = 17 mice. (**P**) Two alternative models illustrating the dependence of neuronal sound responses on normalized pupil diameter. Left: A model in which neuronal habituation depends on the decrease in arousal level. Right: A model in which neuronal habituation is independent of arousal level. Individual dots represent trials. Black: Day 1 trials. Red: Day 5 trials. Lines indicate regression lines. (**Q**) Experimental data showing neuronal response magnitudes binned by normalized pupil diameter separately for Day 1 (black) and Day 5 (red). Day 5 neuronal responses are smaller than Day 1 responses regardless of normalized pupil diameter. Day 1 vs. Day 5: $^{****}P = 2.0 \times 10^{-30}$ (unbalanced two-way ANOVA).

To assess the contribution of global neuromodulation to sensory habituation, we monitored pupil diameter during calcium imaging in a subset of experiments. Pupil diameter showed a gradual decrease across days, providing evidence of habituation in arousal responses (Fig. 1, N and O). However, two observations argued against the possibility that the A1 neuronal habituation stemmed from a general decrease in responsiveness due to lowered arousal. First, plots of trial-to-trial variability of neural activity against pupil diameter showed a distinct separation between Day 1 and Day 5 data regardless of pupil diameter, demonstrating that across-day habituation is independent of arousal levels (Fig. 1, P and Q). Second, independent calcium imaging using two different tone frequencies confirmed the sound specificity of A1 sensory habituation (fig. S3). These data suggest that sensory habituation in A1 is due to sound-specific plasticity rather than global brain state changes. Additionally, we previously found that across-day habituation under these conditions is not inherited from subcortical pathways, as the plasticity was evident in L2/3 but not in the input layer, L4 (*40*). Therefore, we focused on across-day

habituation for the rest of our analyses to determine its cortical circuit mechanisms.

Both the predictive negative image hypothesis and the novelty hypothesis involve the active recruitment of inhibitory neurons during habituation. Since VIP cell activity had not been previously monitored in A1 during across-day habituation, we performed cell type-selective calcium imaging of three inhibitory neuron subclasses—SST cells, VIP cells, and parvalbumin-expressing neurons (PV cells)—to determine their dynamics over five days. We targeted GCaMP6s to each cell type by injecting a conditional GCaMP6s-expressing virus in Cre transgenic mice. Throughout the five-day sound exposure, L2/3 VIP and PV cells exhibited neural habituation similar to pyramidal cells (fig. S4). Interestingly, SST cells showed clear heterogeneity (*48*); deep (>200 μm from the surface) SST neurons showed habituation similar to pyramidal cells, while superficial (<200 μm) neurons exhibited the opposite pattern (*40*, *41*). These findings suggest the involvement of the superficial SST cells in sensory habituation, consistent with the inhibitory dynamics proposed in both theories. However, they do not conclusively support one hypothesis over the other, prompting further investigation into the modulation source for A1 inhibitory neurons.

OFC inactivation reverses sensory habituation in A1

We therefore sought to identify the source of top-down input regulating A1 neuronal activity (Fig. 2A). First, we performed anatomical tracing. After mapping auditory cortices with intrinsic signal imaging, we injected a retrograde tracer into A1 L2/3 (Fig. 2B). Consistent with previous studies, we found many presynaptic neurons in the OFC (*49–52*), secondary motor cortex (M2)(*53–55*), and anterior cingulate cortex (ACC)(*56*) (Fig. 2, C and D), with the ventrolateral and lateral OFC (hereafter, jointly called OFCvl) showing the densest inputs. The lack of overlap between the tracer and VGAT expression indicated that the top-down projections from OFCvl were glutamatergic (fig. S5, A to D). Cell type-selective retrograde tracing with rabies virus further confirmed that both SST and VIP cells receive

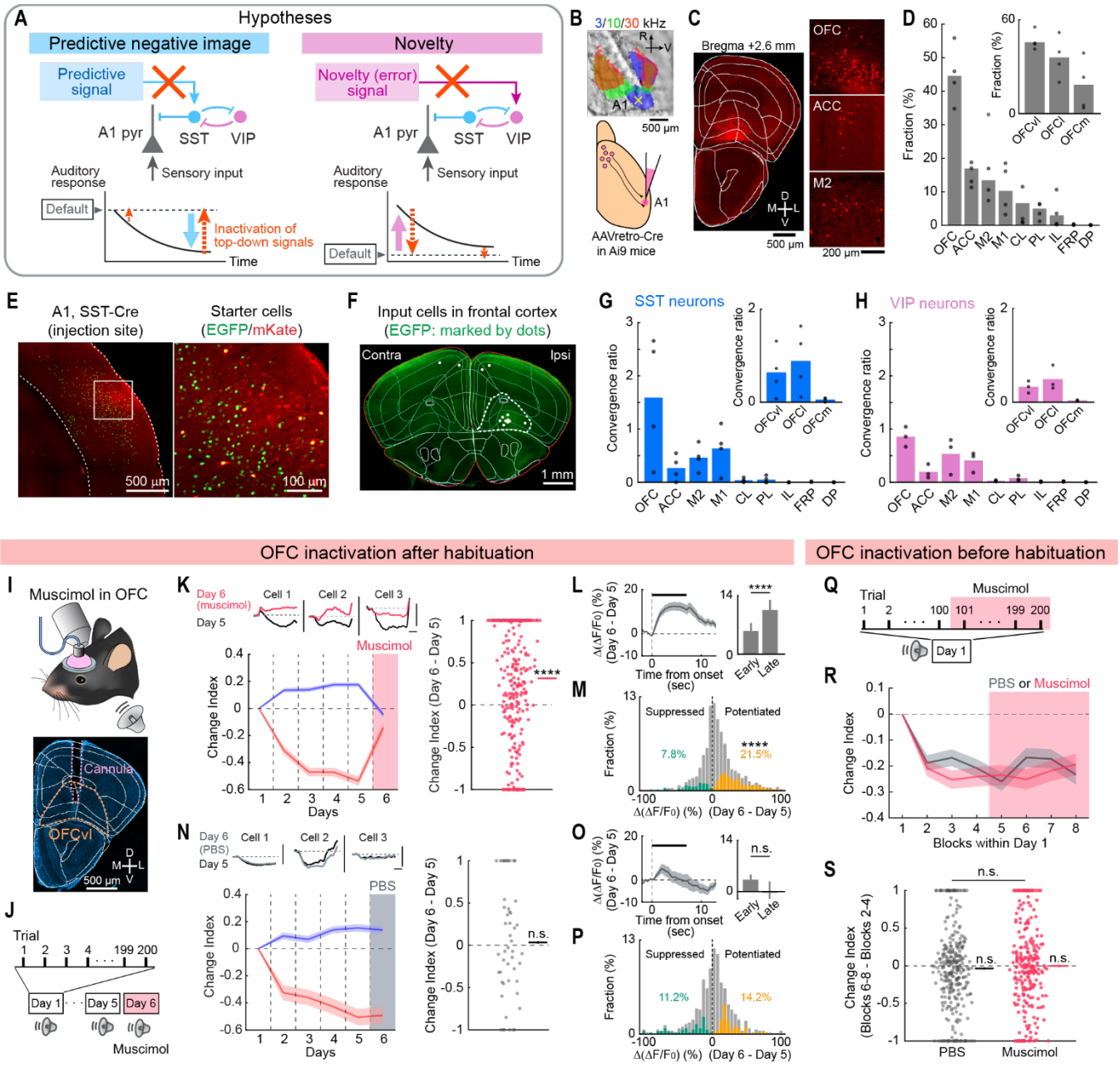

Fig. 2. Inactivation of OFC reverses across-day habituation in A1. (**A**) Schematics illustrating two theories explaining how to distinguish top-down predictive mechanisms from novelty mechanisms. (**B**) Top: Intrinsic signal imaging of pure tone responses superimposed on the cortical surface imaged through the skull. Yellow cross: injection site. Bottom: Schematic illustrating retrograde tracing from A1 L2/3. (**C**) tdTomato-expressing input neurons onto A1 L2/3. Left: Coronal section of the frontal areas overlaid with area borders. Right: Magnified images of OFC, ACC, and M2 areas. (**D**) Bar plots summarizing the distribution of input cells in ipsilateral frontal cortical areas. M1: primary motor cortex, CL: claustrum, DP: dorsal peduncular area. Inset: Further classification of OFC into ventrolateral (OFCvl), lateral (OFCl), and medial (OFCm) subdivisions. *n* = 4 mice. (**E-G**) Retrograde tracing from A1 L2/3 pyramidal neurons using SST-Cre mice. (**E**) Left: Coronal section of the injection site in A1. Dotted lines: cortical borders. Right: Magnified view

of the area indicated by a square in the left image. (**F**) Coronal section of the frontal areas overlaid with area borders. White dots: presynaptic neurons. (**G**) Bar plots summarizing the distribution of input cells in ipsilateral frontal cortical areas. *n* = 4 mice. Inset: Further classification of OFC into ventrolateral (OFCvl), lateral (OFCl), and medial (OFCm) subdivisions. (**H**) Same as (G) but for VIP-Cre mice. (**I**) Top: Schematic illustrating muscimol infusion. Bottom: DAPI-counterstained coronal section showing the cannula implantation site in OFC. (**J**) Protocol for muscimol infusion after habituation. (**K**) Top left: Trial-averaged sound-evoked response traces from three cells. Bottom left: Change Index across days. Pink shade: Muscimol infusion. *n* = 7 mice, 1,392 neurons. Right: Change Index of excitatory responses in individual neurons on Day 6 compared to Day 5 across all mice. *n* = 296 significantly excited neurons. ****$P = 7.9 \times 10^{-16}$ (two-sided Wilcoxon signed-rank test). (**L**) Left: Change in sound-evoked response traces from Day 5 to Day 6, averaged across all significantly excited cells. Right: The amplitudes of the difference trace at 1 and 7 seconds after sound onset. ****$P = 3.4 \times 10^{-7}$. (**M**) Histograms of changes in response magnitudes in all neurons. ****$P = 5.7 \times 10^{-25}$. (**N-P**) The same as (K-M), but for control PBS infusion experiments. (**N**) *n* = 3 mice, 482 total neurons, 49 significantly excited neurons. *P* = 0.52. (**O**) *P* = 0.23. (**P**) *P* = 0.19. (**Q**) Schematic illustrating muscimol infusion in naïve mice. (**R**) Change Index for excitatory responses across blocks of trials. Each data point represents a block of 25 trials. Red: muscimol (*n* = 4 mice). Dark gray: PBS control (*n* = 6 mice). (**S**) Change Index of excitatory responses in individual neurons in blocks 6–8 compared to blocks 2–4 across all mice. *n* = 301 and 242 significantly excited neurons for PBS and muscimol. PBS: *P* = 0.67 (two-sided Wilcoxon signed-rank test), muscimol: *P* = 0.23, PBS vs. muscimol: *P* = 0.49 (two-sided Wilcoxon rank-sum test).

extensive top-down inputs from OFCvl (Fig. 2, E to H, and fig. S6; see Discussion). In contrast, tracer signals in adjacent areas, such as the frontal pole (FRP), prelimbic area (PL), and infralimbic area (IL), were weaker in both AAV and rabies tracing, indicating highly specific wiring of auditory circuits in the frontal cortex (*57–59*).

We next asked whether the frontal top-down input causally contributes to A1 sensory habituation. Two hypotheses predict distinct outcomes with the removal of top-down input (Fig. 2A, red dotted arrows). According to the predictive negative image model, removing the predictive signal should increase sensory responses following habituation but have minimal impact on naïve animals. Conversely, the novelty model suggests that eliminating the novelty signal would diminish sensory responses in naïve animals but have little effect after habituation. To test these predictions, we targeted the OFCvl for pharmacological inactivation, given its strongest top-down connection to A1. After five days of tone habituation, we inactivated OFCvl on Day 6 by infusing muscimol through a pre-implanted

cannula (2.5 mg/mL, 500 nL, 100 nL/min) (Fig. 2, I and J). Remarkably, OFCvl inactivation reversed the sensory habituation in A1 pyramidal cells by enhancing excitatory responses and reducing suppression responses, an effect not observed with the control PBS infusion (Fig. 2, K to P, and fig. S7) (Change Index from Day 5 to Day 6, muscimol: 0.31 ± 0.04, $P = 7.9 \times 10^{-16}$; control: 0.034 ± 0.094, $P =$ 0.52). In a separate experiment, we evaluated the effects of OFCvl inactivation in naïve animals by infusing muscimol on Day 1 (Fig. 2Q). Unlike the post-habituation inactivation, OFCvl inactivation prior to habituation did not alter tone responses (Fig. 2, R and S) (Change Index before and after infusion, muscimol: -0.002 ± 0.017, $P = 0.23$; control: -0.037 ± 0.015, $P = 0.67$). The absence of enhanced responses by muscimol in naïve animals rules out the role of OFCvl in transmitting novelty signals or modulating general sensory processing in A1. Instead, our findings demonstrate the causal role of the OFC specifically in the expression of long-term sensory habituation, aligning with the predictive negative image hypothesis.

Given the involvement of specific inhibitory neuron subtypes in both hypotheses, we further assessed whether inhibitory neurons follow the predictions of these models. We repeated the same six-day OFCvl inactivation experiment while performing cell type-selective imaging of SST, VIP, and PV cells (Fig. 3A). Upon OFCvl inactivation in habituated mice, sound responses in SST cells were significantly reduced (Change Index from Day 5 to Day 6, -0.50 ± 0.06, $P = 1.6 \times 10^{-9}$), as expected from the predictive negative image hypothesis (Fig. 3, B to E). In contrast, both VIP and PV cells showed a marked enhancement in their sound responses, consistent with the release from SST cell-mediated inhibition (PV: 0.18 ± 0.06, $P = 0.036$; VIP: 0.55 ± 0.10, $P = 0.0012$) (Fig. 3, F to M, and fig. S7). These findings further support that the predictive signals from the OFC activate SST cells to suppress other A1 cell types after habituation.

Interestingly, while the effects of both sensory habituation (Fig. 1, G, L, and M) and OFCvl

231 inactivation (Fig. 2, L, Fig. 3, D, H, and L, and fig. S7, E and F) were evident at sound onset (0–1 sec
232 from the tone start), they were significantly more pronounced during the sustained sound stimulus. This
233 slow kinetics of sensory habituation aligns with the recruitment of a long-distance top-down feedback
234 loop and supports the role of prediction, as the sustained phase of the sound is more predictable than the
235 onset.

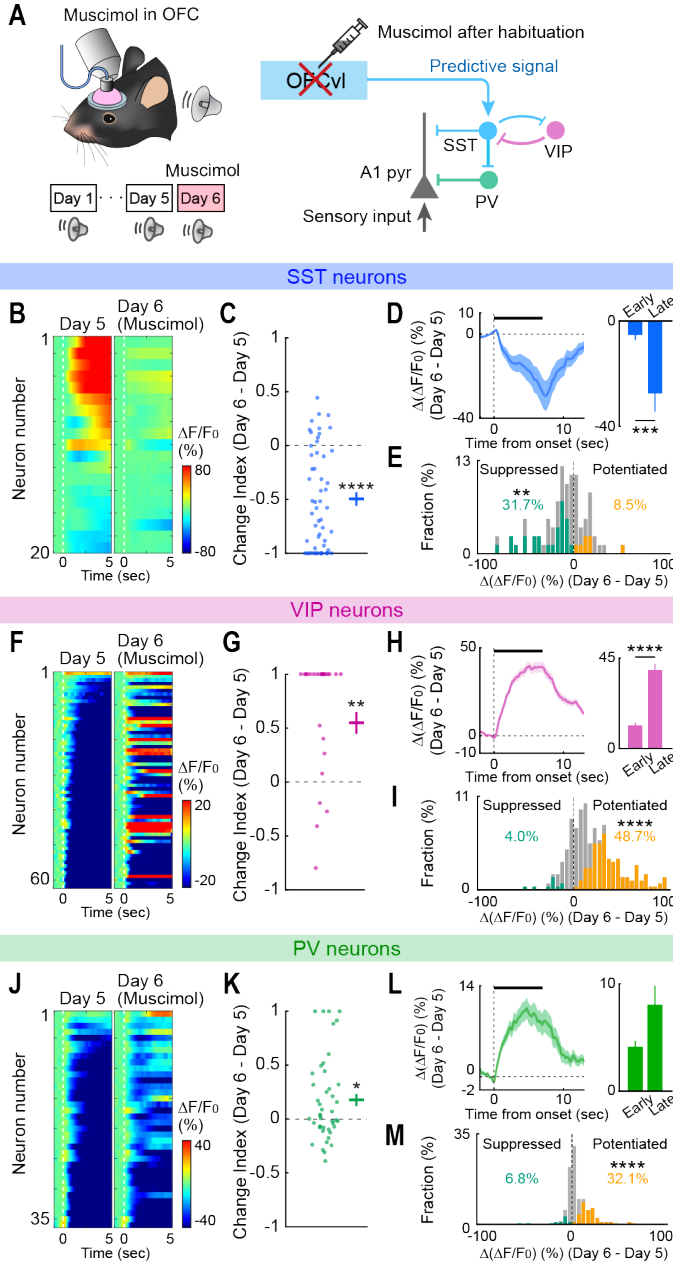

Fig. 3. Post-habituation inactivation of OFC suppresses SST neuron activity in A1. (**A**) Left: Schematic illustrating muscimol infusion after habituation. Right: Circuit diagram of inhibitory neuron connectivity in A1. (**B**) Heatmaps of sound-evoked responses in SST neurons imaged across Days 5 and 6 in a representative mouse. Neurons are sorted by their responses on Day 5. (**C**) Change Index of excitatory responses in individual SST neurons on Day 6 compared to Day 5 across all mice. Lines on the right represent mean ± SEM. n = 4 mice, 54 excited cells. ****P = 1.6 × 10^{-9} (two-sided Wilcoxon signed-rank test). (**D**) Left: Change in sound-evoked response traces from Day 5 to Day 6 averaged across all significantly excited SST cells. Solid line: average. Shading: SEM. Bar, sound. Right: The amplitudes of the difference trace at 1 and 7 seconds after sound onset. ***P = 4.7×10^{-4} (two-sided Wilcoxon signed-rank test). (**E**) Histograms of changes in response magnitudes in all SST neurons. Orange and green bars show neurons with significant increase and decrease. **P = 0.0039 (Fisher's exact test). (**F-I**) Same as (B-E) but for VIP neurons. (**G**) n = 4 mice, 26 excited cells. **P = 0.0012 (**H**) ****P = 3.3 × 10^{-26}. (**I**) ****P = 3.3 × 10^{-36}. (**J-M**) Same as (B-E) but for PV neurons. (**K**) n = 5 mice, 90 excited cells. ****P = 7.9 × 10^{-6}. (**L**) P = 0.30. (**M**) ****P = 4.2 × 10^{-5}.

OFC top-down projection conveys predictive signals and suppresses A1

The OFC plays critical roles in various cognitive functions and has extensive connections with multiple brain regions, including the mediodorsal thalamus, striatum, amygdala, ACC, insular cortex, and sensory cortical areas (*60*). We next investigated whether the direct projection from OFCvl to A1 (fig. S5, E to H) conveys predictive signals during sensory habituation (Fig. 4A).

We visualized sound-evoked activity in the OFCvl→A1 direct pathway by virally expressing axonGCaMP6s in OFCvl neurons. We performed two-photon calcium imaging of their axon terminals in L1 and superficial L2/3 of A1 to track the activity from the same axon boutons over a five-day habituation period (Fig. 4B). On Day 1, significant tone-evoked excitation was observed in 5.5% of axon boutons, consistent with the significant but sparse sound responses previously reported in OFC of naïve mice (*49*, *61*) (Fig. 4, C and D). The sound responses are likely conveyed through the anatomical projections from the auditory cortex to the OFCvl (fig. S5, I to O). However, following habituation, the proportion of excited boutons more than doubled to 13.2%. In axon boutons identified across days, we observed a gradual increase in response magnitudes (Fig. 4, C and E). This increase in OFCvl→A1 axonal activity was more pronounced during the sustained phase of tones (Fig. 4F), consistent with the slow kinetics of habituation in A1 neurons (Fig. 1G, and Fig. 3, D, H, and L). Moreover, this plasticity was specific to the habituated tone frequency, ruling out a general increase in OFCvl responsiveness (Fig. 4, G and H). These results support the hypothesis that the OFC gradually forms an internal model of repeated stimuli, and its direct projection to A1 carries predictive signals that grow over days to recruit SST inhibitory neurons.

Next, we examined whether the increase in the representation of habituated sounds is specific to the OFCvl. Previous research found predictive filtering of A1 responses to self-generated sounds by M2→A1 top-down input (*53*–*55*). Thus, predictive filtering of sensory responses may be a general

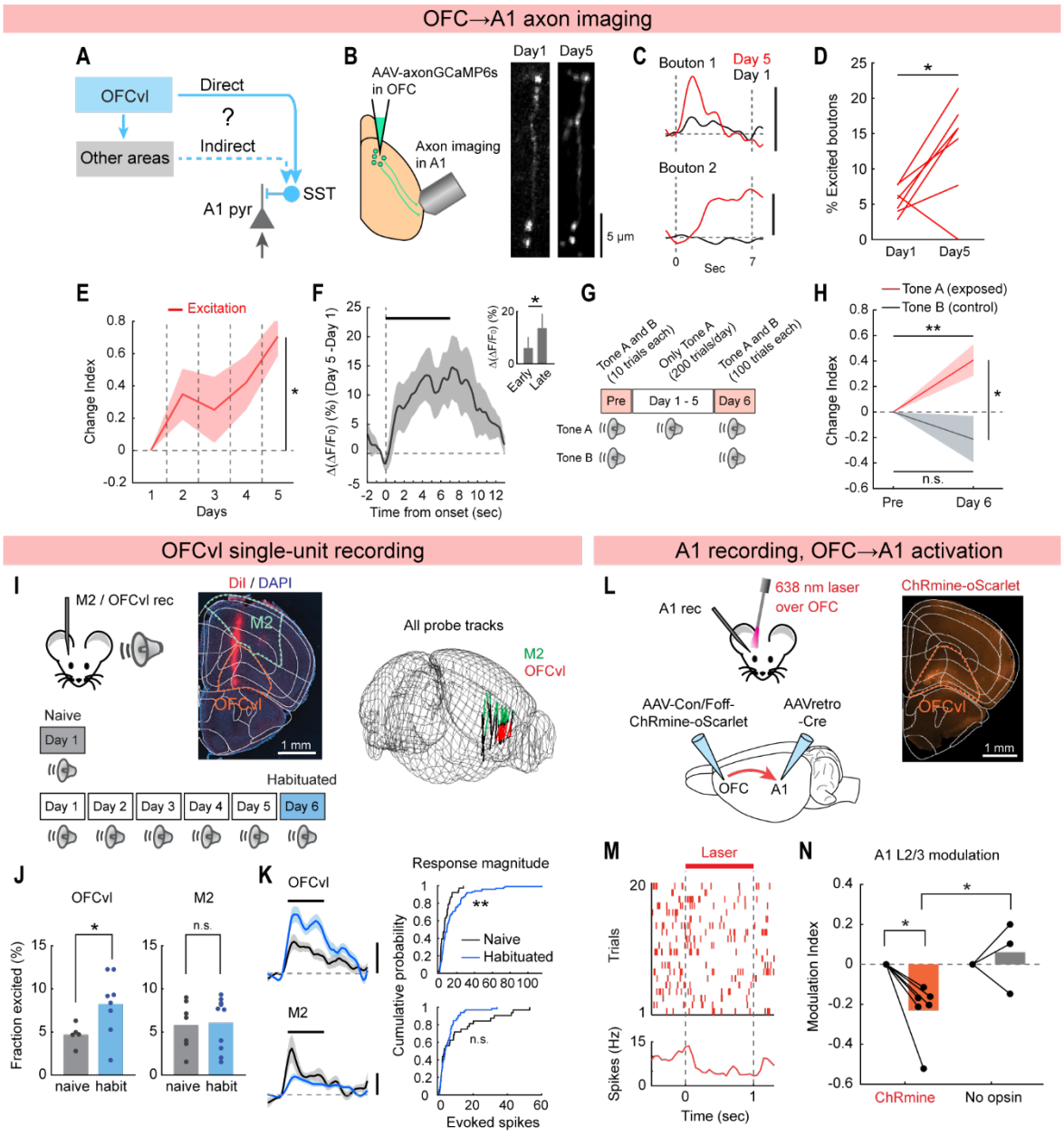

Fig. 4. OFC top-down projection conveys predictive signals and suppresses A1. (**A**) Schematic illustrating direct and indirect pathways from OFC to A1. (**B**) Left: Schematic illustrating projection-specific calcium imaging of the OFC→A1 direct pathway. Right: Representative two-photon image of a GCaMP6s-expressing OFC axon in A1 on Day 1 and Day 5. (**C**) Trial-averaged sound-evoked response traces from two axon boutons. Black: Day 1. Red: Day 5. Scale bar: 50% ΔF/F. Dotted lines indicate sound onset and offset. (**D**) Fraction of boutons with significant excitatory responses on Day 1 and Day 5 across mice. *n* = 7 mice, 326 boutons. **P* = 0.039 (two-sided Wilcoxon signed-rank test). (**E**) Average (solid line) and SEM (shading) of the Change Index for excitatory responses across days. **P* = 0.016 (Day 1 vs. Day 5, two-sided Wilcoxon signed-rank test) (**F**) Change in sound-evoked response traces from Day 1 to Day 5 averaged across all significantly excited boutons. Black bar: sound. Inset shows the amplitudes of the difference trace at 1 and 7 seconds after sound onset. **P* = 0.044 (two-sided Wilcoxon signed-rank test). (**G**) Schematic illustrating the

sound-specific habituation paradigm using two sound frequencies. (**H**) Change Index of excitatory responses to Tone A (habituated) and Tone B (control) on Day 6 compared to the pre-habituation block. *n* = 7 mice, 18 and 13 significantly excited boutons for tones A and B. Tone A: ***P* = 0.0046 (two-sided Wilcoxon signed-rank test, Tone B: *P* = 0.20, Tone A vs. B: **P* = 0.025 (two-sided Wilcoxon rank-sum test). (**I**) Left: Schematic illustrating single-unit recordings in M2 and OFC of naïve and habituated mice. Middle: Coronal section showing the Neuropixels probe track (indicated by DiI) targeting M2 and OFC. The section was counter-stained with DAPI and overlaid with area borders. Right: Summary of all penetrations aligned to the Allen Common Coordinate Framework. Probe tracks within M2 and OFC are shown in green and red, respectively. *n* = 20 penetrations in 17 mice. (**J**) Fraction of single units in OFCvl (left) and M2 (right) with significant excitatory responses in naïve and habituated mice. OFCvl naïve: *n* = 5 mice, habituated: *n* = 7 mice, **P* = 0.045. M2 naïve: *n* = 7 mice, habituated: *n* = 10 mice, *P* = 0.83 (two-sided Wilcoxon rank-sum test). (**K**) Left: Sound-evoked response traces averaged across all significantly excited single units in OFCvl (top) and M2 (bottom) of naïve (black) and habituated (blue) mice. Right: Cumulative plots of sound-evoked spike counts in all significantly excited single units for OFCvl (top) and M2 (bottom). OFCvl, naïve: n = 38 units, habituated: n = 99 units, ***P* = 0.010. M2, naïve: *n* = 32 units, habituated: n = 66 units, *P* = 0.55. (**L**) Left: Schematic illustrating the intersectional strategy to express ChRmine selectively in A1-targeting OFC neurons. Right: Coronal section showing the expression of ChRmine-oScarlet. (**M**) Raster (top) and peristimulus time histogram (bottom) of a representative single unit in A1. (**N**) Modulation Index of A1 L2/3 neural activity by transcranial photostimulation of OFC with a red laser. ChRmine: *n* = 6 mice, *P* = 0.012 (two-sided Wilcoxon signed-rank test). No opsin control: *n* = 3 mice, *P* = 0.67. ChRmine vs. no opsin: *P* = 0.034 (two-sided Wilcoxon rank-sum test).

function shared equally across frontal cortical areas. Alternatively, distinct frontal regions might apply unique filters on A1 activity, tailored to different types of predictions: OFC for predictions based on a history of experiences, and M2 for predictions related to motor corollary discharges.

To investigate these possibilities, we directly compared tone-evoked activities between OFCvl and M2 neurons within the same animals. We performed single-unit recordings using a Neuropixels 1.0 probe that penetrated both regions (Fig. 4I). When we compared tone responses between naïve and habituated mice, we found a 1.7-fold larger fraction of significantly excited OFCvl single units in habituated mice (habituated: 8.2%; naïve: 4.7%, *P* = 0.045), while M2 single-units showed no difference (habituated: 6.1%; naïve: 5.8%, *P* = 0.83) (Fig. 4J). Sound-evoked response magnitudes averaged across all excited single-units showed a significant increase after habituation in OFCvl (104% increase; *P* = 0.010; Fig. 4K). In contrast, M2 units showed a tendency for reduced activity, likely reflecting a weaker

input from the habituated auditory cortex (47% reduction; $P = 0.55$). Recordings in other frontal regions also showed no signs of increased tone responses (fig. S8, A to F). This OFCvl-specific plasticity is consistent with the OFCvl→A1 axonal imaging data and supports a division of labor between OFC and M2 in the predictive filtering of A1 activity across different contexts.

To determine whether activation of the OFCvl→A1 pathway is sufficient to suppress A1 neuronal activity, we next performed pathway-selective optogenetic activation. We restricted the expression of red-shifted opsin ChRmine in A1-projecting OFCvl neurons by an intersectional viral approach (Fig. 4L). Transcranial illumination of the frontal cortex with a red laser successfully evoked action potentials in ChRmine-expressing OFCvl neurons (fig. S8, G and H)(*62*, *63*). A1 recording during activation of OFCvl→A1 pathway revealed significant suppression of A1 activity, an effect absent in control mice without opsin expression (Modulation Index, ChRmine: −0.23 ± 0.06, $P = 0.012$; Control: 0.05 ± 0.07, $P = 0.668$; ChRmine vs. Control: $P = 0.034$; Fig. 4, M and N). Together, these results indicate that the OFCvl stores the information of repeated sensory stimuli and directly transmits predictive signals to A1, triggering neural habituation in A1.

Plasticity in SST cells amplifies sensory habituation

Our results have demonstrated neural plasticity in the OFC, leading to the predictive filtering of A1 sensory responses. However, the OFC is considered to support flexible learning not only through its own plasticity (*64–67*) but also by driving plasticity in other brain regions (*68–71*). A previous study found that pairing OFC→A1 axon terminal activation with tone presentations results in plastic changes in A1 that suppress its responses to the paired frequency (*49*). Therefore, we wondered whether the enhanced OFCvl→A1 input during habituation triggers synaptic plasticity in A1 to further amplify sensory habituation.

We first explored the involvement of overall A1 synaptic plasticity in sensory habituation through the area-selective knockout of N-methyl-D-aspartate (NMDA) receptors. We co-injected AAV9-GCaMP6s and AAV8-mCherry-Cre into the A1 of floxed GluN1 mice ($Grin1^{flox/flox}$) (Fig. 5A). Previous studies using the same mouse showed that Cre-dependent knockout of NMDA receptors became evident within two weeks post-transfection and grew over subsequent weeks (*72–74*). Five weeks post-injection, tone response magnitudes of A1 pyramidal cells were smaller in GluN1 knockout mice compared to control mice (See Methods) (fig. S9, A to D), consistent with the loss of NMDA receptors. Comparing five-day sensory habituation of GluN1 knockout mice to controls revealed a significant reduction in across-day sensory habituation (Fig. 5B), suggesting that local synaptic plasticity in A1 amplifies long-term sensory habituation.

Finally, we focused on synaptic plasticity specifically in SST cells. Given that GluN1 is also expressed in SST cells and regulates their plasticity (*75*, *76*), we generated $Grin1^{flox/flox}$ mice carrying SST-Cre to delete GluN1 selectively in SST cells. A1 pyramidal cells in these mice showed normal tone response properties in a naïve condition (fig. S9, H to K). However, quantification of tone responses across days revealed a significantly diminished habituation in SST cell GluN1 knockout mice compared to the control group (Fig. 5, C and D). In contrast, selective deletion of GluN1 in VIP cells did not affect sensory habituation (Fig. 5, E to G). Thus, while GluN1 deletion in SST cells does not alter basal sound processing in A1, it attenuates sensory habituation through decreased synaptic plasticity. Collectively, our experiments demonstrate that experience-dependent plasticity in both OFCvl circuits and A1 SST cells leads to sensory habituation via the recruitment of SST inhibitory circuits by top-down predictive signals.

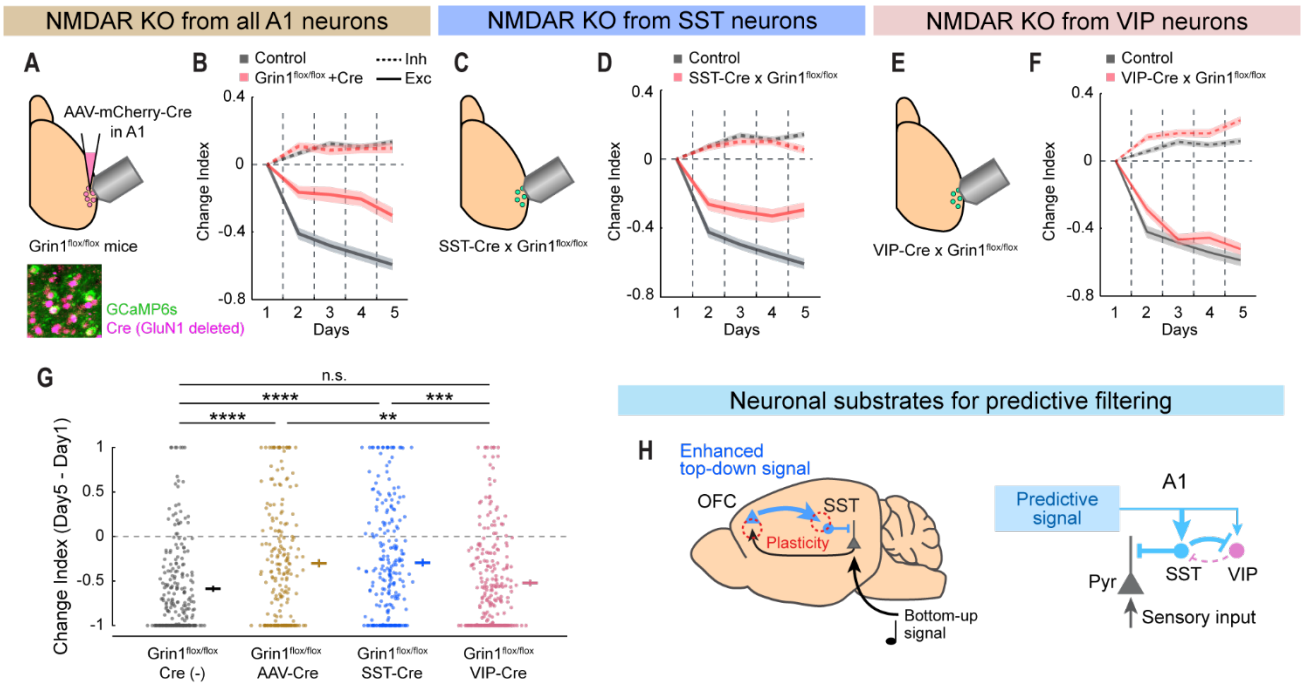

Fig. 5. NMDA receptors in A1 and SST cells are required for habituation. (**A**) Top: Schematic illustrating the viral strategy to knock out NMDA receptors in A1 neurons. Bottom: Representative two-photon image of A1 L2/3 neurons from a Grin1$^{flox/flox}$ mouse expressing GCaMP6s (green) and Cre (red). (**B**) Change Index for excitatory (solid line) and inhibitory (dotted line) sound-evoked responses across days in Grin1$^{flox/flox}$ (red) and control (black) mice. Grin1$^{flox/flox}$: *n* = 4 mice, 905 cells. Control: *n* = 5 mice, 1,708 cells. (**C-D**) Same as (a-b) but for knockout of NMDA receptors selectively in SST neurons. (**E**) SST-Cre × Grin1$^{flox/flox}$: *n* = 5 mice, 1,364 cells. Control: *n* = 6 mice, 1,740 cells. (**E-F**) Same as (a-b) but for knockout of NMDA receptors selectively in VIP neurons. (**F**) VIP-Cre × Grin1$^{flox/flox}$: *n* = 4 mice, 996 cells. Control: *n* = 5 mice, 1,494 cells. (**G**) Summary scatter plots showing the Change Index of excitatory responses in individual neurons on Day 5 compared to Day 1. Grin1$^{flox/flox}$, Cre^{-} control (Ctrl): *n* = 226 excited cells. Grin1$^{flox/flox}$ + AAV-Cre (KO$_{A1}$): *n* = 210. SST-Cre × Grin1$^{flox/flox}$ (KO$_{SST}$): *n* = 231. VIP-Cre × Grin1$^{flox/flox}$ (KO$_{VIP}$): *n* = 254. Ctrl vs. KO$_{A1}$: ****P = 6.9 × 10^{-5}. Ctrl vs. KO$_{SST}$: ****P = 3.2 × 10^{-7}. Ctrl vs. KO$_{VIP}$: P = 1.0. KO$_{A1}$ vs. KO$_{SST}$: P = 1.0. KO$_{A1}$ vs. KO$_{VIP}$: **P = 0.0034. KO$_{SST}$ vs. KO$_{VIP}$: ***P = 3.2 × 10^{-4}. (two-sided Wilcoxon rank-sum test with Bonferroni correction). (**H**) Summary diagrams of sensory habituation pathways.

Discussion

Theories based on human psychophysics have suggested the role of internal predictive models in sensory habituation (fig. S1). Our findings identify the neural substrates for these predictive models and the negative images of sensory stimuli they generate. In naïve animals, bottom-up sensory signals evoke strong responses in the A1. However, with repeated exposure to the same sound over days, a predictive

model forms in the OFC. The OFC then sends top-down predictive signals to SST cells in the A1, which in turn suppress the activity of pyramidal, VIP, and PV cells. This finding may appear at odds with the focus of previous studies on the top-down regulation of VIP cells and the recruitment of the VIP→SST disinhibitory circuit (*48*, *77*, *78*). However, quantification of cell type-specific retrograde tracing from sensory cortical areas has revealed denser top-down connectivity from frontal cortical areas to SST than VIP cells (*52*) (fig. S6). Furthermore, SST and VIP cells are known to form a mutual inhibitory loop (*79–81*), with SST→VIP connections exhibiting one of the highest connection probabilities, largest IPSP amplitudes, and strongest facilitation within cortical circuits (*82*). Therefore, it is not unexpected that top-down input from OFCvl, which connects to both SST and VIP cells, could engage the often overlooked SST→VIP inhibitory connection to suppress the A1 circuit. Synaptic plasticity in SST neurons may further shift the balance of SST-VIP mutual inhibition toward SST dominance to facilitate habituation (Fig. 5H). Our model successfully explains recent studies in V1 that identified a VIP-dominant disinhibitory circuit during animals' first encounter with novel stimuli (*43*, *44*, *83*). We do not exclude the roles of novelty or prediction error signals in other contexts (Supplementary Discussion). However, our data indicate that daily sensory habituation is mediated by an increase in predictive signals, rather than a decrease in novelty (prediction error) signals. Thus, plasticity in the OFC, through the accumulation of experiences over extended periods (*64–67*), creates and updates the internal predictive model of the sensory environment, which is then used to filter neural activity in sensory cortices.

The OFC is considered to support flexible behaviors by encoding the values of predicted outcomes (*84–86*), assigning prediction error credits to corresponding actions (*87*), and tracking associative relationships between stimuli (*1*, *2*, *69*, *88*). However, the extent to which the OFC's top-down projections influence sensory processing remains debated (*49*, *50*, *68*, *89*). Our finding of the OFC's role

391 in the predictive filtering of sensory inputs aligns with the concept that the OFC constructs and uses
392 internal associative models, or "cognitive maps," which dictate predictive relationships between the
393 sensory task space and possible outcomes (*1*, *2*). Furthermore, our results suggest a more generalized
394 function of the OFC beyond merely predicting explicitly rewarding or punishing action outcomes,
395 extending to the attenuation of salience in neutral stimuli during passive experiences. This broader role
396 is reminiscent of the OFC's involvement in "devaluation," where initially favorable stimuli lose their
397 value with satiety or new associations with unfavorable outcomes (*90–92*). It is plausible that sensory
398 inputs inherently carry behavioral values, as they may signal the approach of rewards or threats crucial
399 for an animal's survival. By forming internal associative models, the OFC "devalues" not only explicitly
400 rewarding stimuli but also neutral sensory inputs without meaningful outcomes, thereby inducing
401 habituation.

402 It is worth pointing out the similarity between our findings and the predictive filtering of self-
403 generated sounds, which has been proposed to involve the top-down pathway from the M2 to the A1
404 after days of movement-sound association (*53*, *54*). These studies suggested the recruitment of PV
405 inhibitory neurons, which broadly scale down the A1 activity during movements. Although exact circuits
406 are different, these findings collectively support a general principle: frontal cortical areas send top-down
407 predictive signals based on days of experience—M2 for movement-related predictions and the OFC for
408 familiarity-based predictions, respectively—to filter predictable sensory inputs. In support of this
409 division of labor, we observed a selective enhancement of sound-evoked activity in the OFC, but not in
410 M2, following sensory habituation. Aside from the predictive coding, previous studies also suggested
411 attentional filtering of A1 activity by the prefrontal cortex (*93–96*). Understanding how individual
412 frontal areas are recruited in specific contexts to apply these appropriate filters would be an important
413 area for future research.

Impaired habituation to repeated stimuli and resultant sensory hypersensitivity are commonly observed in mental disorders such as obsessive-compulsive disorders (*4*, *5*) and ASD (*7–10*). Although theories have proposed that a lack of predictive filtering may be central to the symptoms associated with ASD (*29–31*), the neural substrates linking altered neural wiring with reduced sensory filtering have remained unclear. Our discovery that top-down projections from the OFC to A1 are essential for auditory habituation provides crucial insights into the circuit mechanisms underlying reduced habituation in individuals with ASD. It is believed that the neocortical network in ASD displays long-range hypoconnectivity, as indicated by less cohesive activity across brain regions and reduced white matter volume (*97–100*). This reduced long-range communication between frontal areas and sensory cortices could therefore be a culprit for the insufficient habituation in these disorders. This general framework of top-down predictive filtering highlights the importance of targeting long-range frontal projections in developing interventions to alleviate sensory pathophysiology.

References:

1. R. Wilson, Y. Takahashi, G. Schoenbaum, Y. Niv, Orbitofrontal Cortex as a Cognitive Map of Task Space. Neuron 81, 267–279 (2014).
2. K. M. Costa, R. Scholz, K. Lloyd, P. Moreno-Castilla, M. P. H. Gardner, P. Dayan, G. Schoenbaum, The role of the lateral orbitofrontal cortex in creating cognitive maps. Nat. Neurosci. 26, 107–115 (2023).
3. N. C. Rust, M. R. Cohen, Priority coding in the visual system. Nat. Rev. Neurosci. 23, 376–388 (2022).
4. T. Y. Podoly, D. S. Derby, A. Ben-Sasson, Sensory over-responsivity and obsessive-compulsive

disorder: Measuring habituation and sensitivity through self-report, physiological and behavioral indices. J. Psychiatr. Res. 149, 266–273 (2022).

5. M. Hallett, Tourette Syndrome: Update. Brain Dev. 37, 651–655 (2015).

6. D. Titone, T. Ditman, P. S. Holzman, H. Eichenbaum, D. L. Levy, Transitive inference in schizophrenia: impairments in relational memory organization. Schizophr. Res. 68, 235–247 (2004).

7. J. A. Guiraud, E. Kushnerenko, P. Tomalski, K. Davies, H. Ribeiro, M. H. Johnson, Differential habituation to repeated sounds in infants at high risk for autism. Neuroreport 22, 845–849 (2011).

8. S. A. Green, L. Hernandez, N. Tottenham, K. Krasileva, S. Y. Bookheimer, M. Dapretto, Neurobiology of Sensory Overresponsivity in Youth With Autism Spectrum Disorders. JAMA psychiatry 72, 778–786 (2015).

9. W. Jamal, A. Cardinaux, A. J. Haskins, M. Kjelgaard, P. Sinha, Reduced Sensory Habituation in Autism and Its Correlation with Behavioral Measures. J. Autism Dev. Disord. 51, 3153–3164 (2021).

10. A. Kolesnik, J. Begum Ali, T. Gliga, J. Guiraud, T. Charman, M. H. Johnson, E. J. H. Jones, Increased cortical reactivity to repeated tones at 8 months in infants with later ASD. Transl. Psychiatry 9, 1–11 (2019).

11. C. H. Rankin, T. Abrams, R. J. Barry, S. Bhatnagar, D. F. Clayton, J. Colombo, G. Coppola, M. A. Geyer, D. L. Glanzman, S. Marsland, F. K. McSweeney, D. A. Wilson, C. F. Wu, R. F. Thompson, Habituation revisited: An updated and revised description of the behavioral characteristics of habituation. Neurobiol. Learn. Mem. 92, 135–138 (2009).

12. R. F. Thompson, Habituation: a history. Neurobiol. Learn. Mem. 92, 127–134 (2009).

13. D. Wilson, C. Linster, Neurobiology of a simple memory. J. Neurophysiol. 100, 2–7 (2008).

14. M. Wehr, A. Zador, Synaptic mechanisms of forward suppression in rat auditory cortex. Neuron 47, 437–445 (2005).

15. R. G. Natan, J. J. Briguglio, L. Mwilambwe-Tshilobo, S. I. Jones, M. Aizenberg, E. M. Goldberg, M. N. Geffen, Complementary control of sensory adaptation by two types of cortical interneurons. Elife 4, e09868 (2015).

16. Y. Ayala, M. Malmierca, Cholinergic Modulation of Stimulus-Specific Adaptation in the Inferior Colliculus. J. Neurosci. 35, 12261–12272 (2015).

17. V. Castellucci, H. Pinsker, I. Kupfermann, E. R. Kandel, Neuronal Mechanisms of Habituation and Dishabituation of the Gill-Withdrawal Reflex in Aplysia. Science 167, 1745–1748 (1970).

18. F. M. Antunes, I. Nelken, E. Covey, M. S. Malmierca, Stimulus-Specific Adaptation in the Auditory Thalamus of the Anesthetized Rat. PLoS One 5, e14071 (2010).

19. M. S. Malmierca, S. Cristaudo, D. Pérez-González, E. Covey, Stimulus-specific adaptation in the inferior colliculus of the anesthetized rat. J. Neurosci. 29, 5483–5493 (2009).

20. N. Ulanovsky, L. Las, I. Nelken, Processing of low-probability sounds by cortical neurons. Nat. Neurosci. 6, 391–398 (2003).

21. N. Ulanovsky, L. Las, D. Farkas, I. Nelken, Multiple time scales of adaptation in auditory cortex neurons. J. Neurosci. 24, 10440–10453 (2004).

22. I. S. Westenberg, G. Paige, B. Golub, N. M. Weinberger, Evoked potential decrements in auditory cortex. I. Discrete-trial and continual stimulation. Electroencephalogr. Clin. Neurophysiol. 40, 337–355 (1976).

23. I. S. Westenberg, N. M. Weinberger, Evoked potential decrements in auditory cortex. II. Critical test for habituation. Electroencephalogr. Clin. Neurophysiol. 40, 356–369 (1976).

24. N. M. Weinberger, Associative representational plasticity in the auditory cortex: Resolving conceptual and empirical problems. Debates Neurosci. 1, 85–98 (2007).

25. R. D. Hall, Habituation of evoked potentials in the rat under conditions of behavioral control. Electroencephalogr. Clin. Neurophysiol. 24, 155–165 (1968).

26. S. F. Cooke, R. W. Komorowski, E. S. Kaplan, J. P. Gavornik, M. F. Bear, Visual recognition memory, manifested as long-term habituation, requires synaptic plasticity in V1. Nat. Neurosci. 18, 262–271 (2015).

27. M. Ramaswami, Network Plasticity in Adaptive Filtering and Behavioral Habituation. Neuron 82, 1216–1229 (2014).

28. P. Sinha, M. M. Kjelgaard, T. K. Gandhi, K. Tsourides, A. L. Cardinaux, D. Pantazis, S. P. Diamond, R. M. Held, Autism as a disorder of prediction. Proc. Natl. Acad. Sci. 111, 15220–

15225 (2014).

29. S. van de Cruys, K. Evers, R. van der Hallen, L. van Eylen, B. Boets, L. de-Wit, J. Wagemans, Precise minds in uncertain worlds: predictive coding in autism. Psychol. Rev. 121, 649–675 (2014).

30. H. Markram, T. Rinaldi, K. Markram, The intense world syndrome – an alternative hypothesis for autism. Front. Neurosci. 1, 77–96 (2007).

31. C. Moore, M. Carlen, U. Knoblich, J. Cardin, Neocortical Interneurons: From Diversity, Strength. Cell 142, 189–193 (2010).

32. K. Markram, H. Markram, The intense world theory - A unifying theory of the neurobiology of autism. Front. Hum. Neurosci. 4, 224 (2010).

33. M. Turatto, F. Bonetti, C. Chiandetti, D. Pascucci, Context-specific distractors rejection: contextual cues control long-term habituation of attentional capture by abrupt onsets. Vis. cogn. 27, 291–304 (2019).

34. W. P. Jordan, H. C. Strasser, L. McHale, Contextual control of long-term habituation in rats. J. Exp. Psychol. Anim. Behav. Process. 26, 323–339 (2000).

35. A. Dissegna, M. Turatto, C. Chiandetti, Context-specific habituation: A review. Animals 11, 1767 (2021).

36. H. K. Kato, M. W. Chu, J. S. Isaacson, T. Komiyama, Dynamic Sensory Representations in the Olfactory Bulb: Modulation by Wakefulness and Experience. Neuron 76, 962–975 (2012).

37. E. N. Sokolov, Higher nervous functions; the orienting reflex. Annu. Rev. Physiol. 25, 545–580 (1963).

38. C. Wacongne, J. P. Changeux, S. Dehaene, A Neuronal Model of Predictive Coding Accounting for the Mismatch Negativity. J. Neurosci. 32, 3665–3678 (2012).

39. A. R. Wagner, “Habituation and memory” in Mechanisms of Learning and Motivation, A. Dickinson, R. A. Boakes, Eds. (Psychology Press, Hillsdale, NJ, 1979).

40. H. K. Kato, S. N. Gillet, J. S. Isaacson, Flexible Sensory Representations in Auditory Cortex Driven by Behavioral Relevance. Neuron 88, 1027–1039 (2015).

41. S. N. Gillet, H. K. Kato, M. A. Justen, M. Lai, J. S. Isaacson, Fear Learning Regulates Cortical

Sensory Representations by Suppressing Habituation. Front. Neural Circuits 11, 112 (2018).

42. H. Makino, T. Komiyama, Learning enhances the relative impact of top-down processing in the visual cortex. Nat. Neurosci. 18, 1116–1122 (2015).

43. M. Garrett, S. Manavi, K. Roll, D. R. Ollerenshaw, P. A. Groblewski, N. D. Ponvert, J. T. Kiggins, L. Casal, K. Mace, A. Williford, A. Leon, X. Jia, P. Ledochowitsch, M. A. Buice, W. Wakeman, S. Mihalas, S. R. Olsen, Experience shapes activity dynamics and stimulus coding of VIP inhibitory cells. Elife 9, e50340 (2020).

44. M. Garrett, P. Groblewski, A. Piet, D. Ollerenshaw, F. Najafi, I. Yavorska, A. Amster, C. Bennett, M. Buice, S. Caldejon, L. Casal, F. D'Orazi, S. Daniel, S. E. de Vries, D. Kapner, J. Kiggins, J. Lecoq, P. Ledochowitsch, S. Manavi, N. Mei, C. B. Morrison, S. Naylor, N. Orlova, J. Perkins, N. Ponvert, C. Roll, S. Seid, D. Williams, A. Williford, R. Ahmed, D. Amine, Y. Billeh, C. Bowman, N. Cain, A. Cho, T. Dawe, M. Departee, M. Desoto, D. Feng, S. Gale, E. Gelfand, N. Gradis, C. Grasso, N. Hancock, B. Hu, R. Hytnen, X. Jia, T. Johnson, I. Kato, S. Kivikas, L. Kuan, Q. L'Heureux, S. Lambert, A. Leon, E. Liang, F. Long, K. Mace, I. M. de Abril, C. Mochizuki, C. Nayan, K. North, L. Ng, G. K. Ocker, M. Oliver, P. Rhoads, K. Ronellenfitch, K. Schelonka, J. Sevigny, D. Sullivan, B. Sutton, J. Swapp, T. K. Nguyen, X. Waughman, J. Wilkes, M. Wang, C. Farrell, W. Wakeman, H. Zeng, J. Phillips, S. Mihalas, A. Arkhipov, C. Koch, S. R. Olsen, Stimulus novelty uncovers coding diversity in visual cortical circuits. bioRxiv, 2023.02.14.528085 (2023).

45. K. Aitken, L. Campagnola, M. E. Garrett, S. R. Olsen, S. Mihalas, Simple synaptic modulations implement diverse novelty computations. Cell Rep. 43, 114188 (2024).

46. J. Homann, S. A. Koay, K. S. Chen, D. W. Tank, M. J. Berry, Novel stimuli evoke excess activity in the mouse primary visual cortex. Proc. Natl. Acad. Sci. U. S. A. 119, e2108882119 (2022).

47. D. P. Narayanan, H. Tsukano, A. M. Kline, K. Onodera, H. K. Kato, Biological constraints on stereotaxic targeting of functionally-defined cortical areas. Cereb. Cortex 33, 3293–3310 (2023).

48. S. Furutachi, A. D. Franklin, T. D. Mrsic-Flogel, S. B. Hofer, Cooperative thalamocortical circuit mechanism for sensory prediction errors. bioRxiv, 2023.07.12.548664 (2023).

49. D. E. Winkowski, D. A. Nagode, K. J. Donaldson, P. Yin, S. A. Shamma, J. B. Fritz, P. O. Kanold, Orbitofrontal Cortex Neurons Respond to Sound and Activate Primary Auditory Cortex Neurons.

Cereb. Cortex 28, 868–879 (2018).

50. D. Winkowski, S. Bandyopadhyay, S. Shamma, P. Kanold, Frontal Cortex Activation Causes Rapid Plasticity of Auditory Cortical Processing. J. Neurosci. 33, 18134–18148 (2013).

51. R. Ying, L. Hamlette, L. Nikoobakht, R. Balaji, N. Miko, M. L. Caras, Organization of orbitofrontal-auditory pathways in the Mongolian gerbil. J. Comp. Neurol. 531, 1459–1481 (2023).

52. G. ichi Tasaka, C. Maggi, E. Taha, A. Mizrahi, The local and long-range input landscape of inhibitory neurons in mouse auditory cortex. J. Comp. Neurol. 531, 502–514 (2023).

53. D. M. Schneider, J. Sundararajan, R. Mooney, A cortical filter that learns to suppress the acoustic consequences of movement. Nature 561, 391–395 (2018).

54. D. M. Schneider, A. Nelson, R. Mooney, A synaptic and circuit basis for corollary discharge in the auditory cortex. Nature 513, 189–194 (2014).

55. A. Nelson, D. Schneider, J. Takatoh, K. Sakurai, F. Wang, R. Mooney, A Circuit for Motor Cortical Modulation of Auditory Cortical Activity. J. Neurosci. 33, 14342–14353 (2013).

56. W. Sun, P. Tang, Y. Liang, J. Li, J. Feng, N. Zhang, D. Lu, J. He, X. Chen, The anterior cingulate cortex directly enhances auditory cortical responses in air-puffing-facilitated flight behavior. Cell Rep. 38, 110506 (2022).

57. S. W. Oh, J. A. Harris, L. Ng, B. Winslow, N. Cain, S. Mihalas, Q. Wang, C. Lau, L. Kuan, A. M. Henry, M. T. Mortrud, B. Ouellette, T. N. Nguyen, S. A. Sorensen, C. R. Slaughterbeck, W. Wakeman, Y. Li, D. Feng, A. Ho, E. Nicholas, K. E. Hirokawa, P. Bohn, K. M. Joines, H. Peng, M. J. Hawrylycz, J. W. Phillips, J. G. Hohmann, P. Wohnoutka, C. R. Gerfen, C. Koch, A. Bernard, C. Dang, A. R. Jones, H. Zeng, A mesoscale connectome of the mouse brain. Nature 508, 207–214 (2014).

58. Allen Institute for Brain Science, Allen Mouse Brain Connectivity Atlas (2011). http://connectivity.brain-map.org/.

59. L. Gao, S. Liu, L. Gou, Y. Hu, Y. Liu, L. Deng, D. Ma, H. Wang, Q. Yang, Z. Chen, D. Liu, S. Qiu, X. Wang, D. Wang, X. Wang, B. Ren, Q. Liu, T. Chen, X. Shi, H. Yao, C. Xu, C. T. Li, Y. Sun, A. Li, Q. Luo, H. Gong, N. Xu, J. Yan, Single-neuron projectome of mouse prefrontal cortex. Nat. Neurosci. 25, 515–529 (2022).

60. C. Cavada, T. Compañy, J. Tejedor, R. J. Cruz-Rizzolo, F. Reinoso-Suárez, The anatomical connections of the macaque monkey orbitofrontal cortex. A review. Cereb. Cortex 10, 220–242 (2000).

61. H. K. Srivastava, S. Bandyopadhyay, Parallel Lemniscal and Non-Lemniscal Sources Control Auditory Responses in the Orbitofrontal Cortex (OFC). eNeuro 7, 1–19 (2020).

62. R. Chen, F. Gore, Q. A. Nguyen, C. Ramakrishnan, S. Patel, S. H. Kim, M. Raffiee, Y. S. Kim, B. Hsueh, E. Krook-Magnusson, I. Soltesz, K. Deisseroth, Deep brain optogenetics without intracranial surgery. Nat. Biotechnol. 39, 161–164 (2021).

63. J. H. Marshel, Y. S. Kim, T. A. Machado, S. Quirin, B. Benson, J. Kadmon, C. Raja, A. Chibukhchyan, C. Ramakrishnan, M. Inoue, J. C. Shane, D. J. McKnight, S. Yoshizawa, H. E. Kato, S. Ganguli, K. Deisseroth, Cortical layer-specific critical dynamics triggering perception. Science 365, eaaw5202 (2019).

64. R. Hattori, N. G. Hedrick, A. Jain, S. Chen, H. You, M. Hattori, J. H. Choi, B. K. Lim, R. Yasuda, T. Komiyama, Meta-reinforcement learning via orbitofrontal cortex. Nat. Neurosci. 26, 2182–2191 (2023).

65. V. M. K. Namboodiri, J. M. Otis, K. van Heeswijk, E. S. Voets, R. A. Alghorazi, J. Rodriguez-Romaguera, S. Mihalas, G. D. Stuber, Single-cell activity tracking reveals that orbitofrontal neurons acquire and maintain a long-term memory to guide behavioral adaptation. Nat. Neurosci. 22, 1110–1121 (2019).

66. A. J. Whyte, H. W. Kietzman, A. M. Swanson, L. M. Butkovich, B. R. Barbee, G. J. Bassell, C. Gross, S. L. Gourley, A. contributions, S. designed research, S. performed research, S. analyzed data, N. Raj, J. Yamin, H. Arrowood, A. Allen, K. Zimmermann, Reward-related expectations trigger dendritic spine plasticity in the mouse ventrolateral orbitofrontal cortex. J. Neurosci. 39, 4595–4605 (2019).

67. C. M. Johnson, H. Peckler, L. H. Tai, L. Wilbrecht, Rule learning enhances structural plasticity of long-range axons in frontal cortex. Nat. Commun. 7, 1–14 (2016).

68. A. Banerjee, G. Parente, J. Teutsch, C. Lewis, F. F. Voigt, F. Helmchen, Value-guided remapping of sensory cortex by lateral orbitofrontal cortex. Nature 585, 245–250 (2020).

69. M. P. H. Gardner, G. Schoenbaum, The orbitofrontal cartographer. Behav. Neurosci. 135, 267–

276 (2021).

70. K. J. Miller, M. M. Botvinick, C. D. Brody, Value representations in the rodent orbitofrontal cortex drive learning, not choice. Elife 11, e64575 (2022).

71. M. Malvaez, C. Shieh, M. D. Murphy, V. Y. Greenfield, K. M. Wassum, Distinct cortical–amygdala projections drive reward value encoding and retrieval. Nat. Neurosci. 22, 762–769 (2019).

72. R. Deng, M. Chang, J. P. Y. Kao, P. O. Kanold, Cortical inhibitory but not excitatory synaptic transmission and circuit refinement are altered after the deletion of NMDA receptors during early development. Sci. Rep. 13, 656 (2023).

73. R. S. Larsen, I. T. Smith, J. Miriyala, J. E. Han, R. J. Corlew, S. L. Smith, B. D. Philpot, Synapse-Specific Control of Experience-Dependent Plasticity by Presynaptic NMDA Receptors. Neuron 83, 879–893 (2014).

74. T. Iwasato, A. Datwani, A. M. Wolf, H. Nishiyama, Y. Taguchi, S. Tonegawa, T. Knöpfel, R. S. Erzurumlu, S. Itohara, Cortex-restricted disruption of NMDAR1 impairs neuronal patterns in the barrel cortex. Nature 406, 726–731 (2000).

75. M. Perez-Rando, E. Castillo-Gómez, R. Guirado, J. M. Blasco-Ibañez, C. Crespo, E. Varea, J. Nacher, NMDA receptors regulate the structural plasticity of spines and axonal boutons in hippocampal interneurons. Front. Cell. Neurosci. 11, 271022 (2017).

76. G. Nyíri, F. A. Stephenson, T. F. Freund, P. Somogyi, Large variability in synaptic n-methyl-d-aspartate receptor density on interneurons and a comparison with pyramidal-cell spines in the rat hippocampus. Neuroscience 119, 347–363 (2003).

77. Y. Fu, J. M. Tucciarone, J. S. Espinosa, N. Sheng, D. P. Darcy, R. A. Nicoll, Z. J. Huang, M. P. Stryker, S. Espinosa, N. Sheng, D. P. Darcy, R. A. Nicoll, J. Huang, M. P. Stryker, A Cortical Circuit for Gain Control by Behavioral State. Cell 156, 1139–1152 (2014).

78. S. Zhang, M. Xu, T. Kamigaki, J. P. H. Do, W.-C. Chang, S. Jenvay, K. Miyamichi, L. Luo, Y. Dan, Long-range and local circuits for top-down modulation of visual cortex processing. Science 345, 660–665 (2014).

79. X. Jiang, S. Shen, C. R. Cadwell, P. Berens, F. Sinz, A. S. Ecker, S. Patel, A. S. Tolias, Principles of connectivity among morphologically defined cell types in adult neocortex. Science 350,

aac9462 (2015).

80. C. K. Pfeffer, M. Xue, M. He, Z. J. Huang, M. Scanziani, Inhibition of inhibition in visual cortex: The logic of connections between molecularly distinct interneurons. Nat. Neurosci. 16, 1068–1076 (2013).

81. M. Karnani, J. Jackson, I. Ayzenshtat, J. Tucciarone, K. Manoocheri, W. Snider, R. Yuste, Cooperative Subnetworks of Molecularly Similar Interneurons in Mouse Neocortex. Neuron 90, 86–100 (2016).

82. L. Campagnola, S. C. Seeman, T. Chartrand, L. Kim, A. Hoggarth, C. Gamlin, S. Ito, J. Trinh, P. Davoudian, C. Radaelli, M. H. Kim, T. Hage, T. Braun, L. Alfiler, J. Andrade, P. Bohn, R. Dalley, A. Henry, S. Kebede, A. Mukora, D. Sandman, G. Williams, R. Larsen, C. Teeter, T. L. Daigle, K. Berry, N. Dotson, R. Enstrom, M. Gorham, M. Hupp, S. D. Lee, K. Ngo, P. R. Nicovich, L. Potekhina, S. Ransford, A. Gary, J. Goldy, D. McMillen, T. Pham, M. Tieu, L. Siverts, M. Walker, C. Farrell, M. Schroedter, C. Slaughterbeck, C. Cobb, R. Ellenbogen, R. P. Gwinn, C. D. Keene, A. L. Ko, J. G. Ojemann, D. L. Silbergeld, D. Carey, T. Casper, K. Crichton, M. Clark, N. Dee, L. Ellingwood, J. Gloe, M. Kroll, J. Sulc, H. Tung, K. Wadhwani, K. Brouner, T. Egdorf, M. Maxwell, M. McGraw, C. A. Pom, A. Ruiz, J. Bomben, D. Feng, N. Hejazinia, S. Shi, A. Szafer, W. Wakeman, J. Phillips, A. Bernard, L. Esposito, F. D. D'Orazi, S. Sunkin, K. Smith, B. Tasic, A. Arkhipov, S. Sorensen, E. Lein, C. Koch, G. Murphy, H. Zeng, T. Jarsky, Local connectivity and synaptic dynamics in mouse and human neocortex. Science 375, eabj5861 (2022).

83. K. Aitken, L. Campagnola, M. Garrett, S. Olsen, S. Mihalas, Familiarity modulated synapses model visual cortical circuit novelty responses. bioRxiv, 2023.08.16.553635 (2023).

84. C. Padoa-Schioppa, J. A. Assad, Neurons in the orbitofrontal cortex encode economic value. Nature 441, 223–226 (2006).

85. J. Hirokawa, A. Vaughan, P. Masset, T. Ott, A. Kepecs, Frontal cortex neuron types categorically encode single decision variables. Nature 576, 446–451 (2019).

86. G. Schoenbaum, A. A. Chiba, M. Gallagher, Orbitofrontal cortex and basolateral amygdala encode expected outcomes during learning. Nat. Neurosci. 1, 155–159 (1998).

87. M. E. Walton, T. E. J. Behrens, M. J. Buckley, P. H. Rudebeck, M. F. S. Rushworth, Separable learning systems in the macaque brain and the role of orbitofrontal cortex in contingent learning.

Neuron 65, 927–939 (2010).

88. G. Schoenbaum, M. R. Roesch, T. A. Stalnaker, Y. K. Takahashi, A new perspective on the role of the orbitofrontal cortex in adaptive behaviour. Nat. Rev. Neurosci. 10, 885–892 (2009).

89. D. Liu, J. Deng, Z. Zhang, Z. Y. Zhang, Y. G. Sun, T. Yang, H. Yao, Orbitofrontal control of visual cortex gain promotes visual associative learning. Nat. Commun. 11, 1–14 (2020).

90. J. D. Howard, T. Kahnt, Identity-Specific Reward Representations in Orbitofrontal Cortex Are Modulated by Selective Devaluation. J. Neurosci. 37, 2627–2638 (2017).

91. M. P. H. Gardner, J. S. Conroy, M. H. Shaham, C. V. Styer, G. Schoenbaum, Lateral Orbitofrontal Inactivation Dissociates Devaluation-Sensitive Behavior and Economic Choice. Neuron 96, 1192-1203.e4 (2017).

92. J. A. Gottfried, J. O'Doherty, R. J. Dolan, Encoding predictive reward value in human amygdala and orbitofrontal cortex. Science 301, 1104–1107 (2003).

93. M. Nakajima, L. I. Schmitt, M. M. Halassa, Prefrontal Cortex Regulates Sensory Filtering through a Basal Ganglia-to-Thalamus Pathway. Neuron 103, 445-458.e10 (2019).

94. J. Fritz, S. Shamma, M. Elhilali, D. Klein, Rapid task-related plasticity of spectrotemporal receptive fields in primary auditory cortex. Nat. Neurosci. 6, 1216–1223 (2003).

95. J. B. Fritz, M. Elhilali, S. A. Shamma, Differential dynamic plasticity of A1 receptive fields during multiple spectral tasks. J. Neurosci. 25, 7623–7635 (2005).

96. J. Fritz, M. Elhilali, S. Shamma, Adaptive changes in cortical receptive fields induced by attention to complex sounds. J. Neurophysiol. 98, 2337–2346 (2007).

97. M. E. Vissers, M. X Cohen, H. M. Geurts, Brain connectivity and high functioning autism: A promising path of research that needs refined models, methodological convergence, and stronger behavioral links. Neurosci. Biobehav. Rev. 36, 604–625 (2012).

98. J. J. Wolff, H. Gu, G. Gerig, J. T. Elison, M. Styner, S. Gouttard, K. N. Botteron, S. R. Dager, G. Dawson, A. M. Estes, A. C. Evans, H. C. Hazlett, P. Kostopoulos, R. C. McKinstry, S. J. Paterson, R. T. Schultz, L. Zwaigenbaum, J. Piven, Differences in white matter fiber tract development present from 6 to 24 months in infants with autism. Am. J. Psychiatry 169, 589–600 (2012).

99. E. Courchesne, K. Pierce, Why the frontal cortex in autism might be talking only to itself: Local

over-connectivity but long-distance disconnection. Curr. Opin. Neurobiol. 15, 225–230 (2005).

100. S. Wass, Distortions and disconnections: Disrupted brain connectivity in autism. Brain Cogn. 75, 18–28 (2011).

101. M. Pachitariu, C. Stringer, M. Dipoppa, S. Schröder, L. F. Rossi, H. Dalgleish, M. Carandini, K. D. Harris, Suite2p: beyond 10,000 neurons with standard two-photon microscopy. bioRxiv, 061507 (2017).

102. M. Pachitariu, N. Steinmetz, S. Kadir, M. Carandini, K. D. Harris, Kilosort: realtime spike-sorting for extracellular electrophysiology with hundreds of channels. bioRxiv, 061481 (2016).

103. C. Rossant, S. Kadir, D. Goodman, J. Schulman, M. Hunter, A. Saleem, A. Grosmark, M. Belluscio, G. Denfield, A. Ecker, A. Tolias, S. Solomon, G. Buzsaki, M. Carandini, K. Harris, Spike sorting for large, dense electrode arrays. Nat Neurosci 19, 634–641 (2016).

104. J. M. J. Fabre, E. H. van Beest, A. J. Peters, M. Carandini, K. D. Harris, Bombcell: automated curation and cell classification of spike-sorted electrophysiology data. Zenodo, doi: 10.5281/ZENODO.8172822 (2023).

105. Y. Senzai, A. Fernandez-Ruiz, G. Buzsáki, Layer-Specific Physiological Features and Interlaminar Interactions in the Primary Visual Cortex of the Mouse. Neuron 101, 500-513.e5 (2019).

106. I. Wickersham, D. Lyon, R. Barnard, T. Mori, S. Finke, K.-K. Conzelmann, J. Young, E. Callaway, Monosynaptic Restriction of Transsynaptic Tracing from Single, Genetically Targeted Neurons. Neuron 53, 639–647 (2007).

107. T. Moser, D. Beutner, Kinetics of exocytosis and endocytosis at the cochlear inner hair cell afferent synapse of the mouse. Proc. Natl. Acad. Sci. U. S. A. 97, 883–888 (2000).

108. J. D. Goutman, Mechanisms of synaptic depression at the hair cell ribbon synapse that support auditory nerve function. Proc. Natl. Acad. Sci. U. S. A. 114, 9719–9724 (2017).

109. K. Meyer, E. M. Rouiller, G. Loquet, Direct comparison between properties of adaptation of the auditory nerve and the ventral cochlear nucleus in response to repetitive clicks. Hear. Res. 228, 144–155 (2007).

110. G. Loquet, E. M. Rouiller, Neural adaptation to pulsatile acoustical stimulation in the cochlear

722 nucleus of the rat. Hear. Res. 171, 72–81 (2002).

723 111. D. Duque, X. Wang, J. Nieto-Diego, K. Krumbholz, M. S. Malmierca, Neurons in the inferior
724 colliculus of the rat show stimulus-specific adaptation for frequency, but not for intensity. Sci.
725 Rep. 6, 1–15 (2016).

726 112. G. G. Parras, J. Nieto-Diego, G. V. Carbajal, C. Valdés-Baizabal, C. Escera, M. S. Malmierca,
727 Neurons along the auditory pathway exhibit a hierarchical organization of prediction error. Nat.
728 Commun. 8, 1–17 (2017).

729 113. L. A. Anderson, G. B. Christianson, J. F. Linden, Stimulus-specific adaptation occurs in the
730 auditory thalamus. J. Neurosci. 29, 7359–7363 (2009).

731 114. R. G. Natan, W. Rao, M. N. Geffen, Cortical Interneurons Differentially Shape Frequency Tuning
732 following Adaptation. Cell Rep. 21, 878–890 (2017).

733 115. G. Keller, T. Bonhoeffer, M. Hübener, Sensorimotor Mismatch Signals in Primary Visual Cortex
734 of the Behaving Mouse. Neuron 74, 809–815 (2012).

735 116. N. J. Audette, W. X. Zhou, A. La Chioma, D. M. Schneider, Precise movement-based predictions
736 in the mouse auditory cortex. Curr. Biol. 32, 4925-4940.e6 (2022).

737 117. R. Näätänen, A. W. K. Gaillard, S. Mäntysalo, Early selective-attention effect on evoked potential
738 reinterpreted. Acta Psychol. (Amst). 42, 313–329 (1978).

739 118. A. M. H. Lesicko, C. F. Angeloni, J. M. Blackwell, M. De Biasi, M. N. Geffen, Cortico-Fugal
740 Regulation of Predictive Coding. Elife 11, e73289 (2022).

741 119. K. Obara, T. Ebina, S. I. Terada, T. Uka, M. Komatsu, M. Takaji, A. Watakabe, K. Kobayashi, Y.
742 Masamizu, H. Mizukami, T. Yamamori, K. Kasai, M. Matsuzaki, Change detection in the primate
743 auditory cortex through feedback of prediction error signals. Nat. Commun. 14, 1–17 (2023).

744 120. A. Hockley, M. S. Malmierca, Auditory processing control by the medial prefrontal cortex: A
745 review of the rodent functional organisation. Hear. Res. 443, 108954 (2024).

746 121. J. H. Sul, H. Kim, N. Huh, D. Lee, M. W. Jung, Distinct Roles of Rodent Orbitofrontal and
747 Medial Prefrontal Cortex in Decision Making. Neuron 66, 449–460 (2010).

748 122. J. P. O'Doherty, P. Dayan, K. Friston, H. Critchley, R. J. Dolan, Temporal Difference Models and
749 Reward-Related Learning in the Human Brain. Neuron 38, 329–337 (2003).

123. A. C. Nobre, J. T. Coull, C. D. Frith, M. M. Mesulam, Orbitofrontal cortex is activated during breaches of expectation in tasks of visual attention. Nat. Neurosci. 2, 11–12 (1999).

124. S. W. Kennerley, A. F. Dahmubed, A. H. Lara, J. D. Wallis, Neurons in the Frontal Lobe Encode the Value of Multiple Decision Variables. J. Cogn. Neurosci. 21, 1162–1178 (2009).

125. Y. K. Takahashi, M. R. Roesch, T. A. Stalnaker, R. Z. Haney, D. J. Calu, A. R. Taylor, K. A. Burke, G. Schoenbaum, The Orbitofrontal Cortex and Ventral Tegmental Area Are Necessary for Learning from Unexpected Outcomes. Neuron 62, 269–280 (2009).

126. T. A. Stalnaker, T. L. Liu, Y. K. Takahashi, G. Schoenbaum, Orbitofrontal neurons signal reward predictions, not reward prediction errors. Neurobiol. Learn. Mem. 153, 137–143 (2018).

127. F. Pouille, M. Scanziani, Routing of spike series by dynamic circuits in the hippocampus. Nature 429, 717–723 (2004).

Acknowledgments: We thank Paul Manis, Jeffry Isaacson, Daniel Polley, and the members of the Kato Lab for their advice throughout the project and comments on the manuscript. We thank Gonçalo Lopes for his support in setting up Bonsai for pupil monitoring.

Funding:

National Institutes of Health grant R01DC017516 (HKK)

National Institute of Health grant RF1NS128873 (HKK)

Simons Foundation (HKK)

Eagles Autism Foundation (HKK)

Foundation of Hope (HKK, HT).

Author contributions:

Conceptualization: HT, HKK

Methodology: HT, MMG, HKK

Investigation: HT, MMG, PRD, HKK

Formal analysis: HT, HKK

Visualization: HT, HKK

Funding acquisition: HT, HKK

Project administration: HKK

Supervision: HKK

Writing – original draft: HT, HKK

Writing – review & editing: HT, MMG, PRD, HKK

Competing interests: The authors declare no competing interests.

Data and materials availability: All data generated in this study will be deposited in the DANDI Archive. Source data for all figures will be provided in this paper as a supplementary data file attached to this paper. Custom Matlab codes used in this study will be made available from the corresponding author upon request.